Chemical Engineering Journal 440 (2022) 135565

Contents lists available at ScienceDirect

Chemical Engineering Journal

journal homepage: www.elsevier.com/locate/cej

Impact of ultrathin coating layer on lithium-ion intercalation into particles for lithium-ion batteries

Yufang He [a], Hiep Pham [a], Xinhua Liang [b], Jonghyun Park [a,*]

[a] Department of Mechanical Engineering and Aerospace Engineering, Missouri University of Science and Technology, Rolla, 65401, USA
[b] Linda and Bipin Doshi Department of Chemical and Biochemical Engineering, Missouri University of Science and Technology, Rolla, 65401, USA

ARTICLE INFO

Keywords:
Atomic layer deposition
Li-ion intercalation
Li-ion diffusivity
Coating volume expansion

ABSTRACT

Ultrathin film coatings on battery materials via atomic layer deposition (ALD) have been demonstrated as an efficient technology for battery performance enhancement. However, the fundamental understanding on lithium intercalation into active materials through the interface between the coating and active materials is unclear, which makes it difficult to optimize ALD coating strategies. Further, like most active materials, a coating layer can undergo volume change during the intercalation process, which can produce detrimental structural changes and mechanical failure of the layer. In this work, first-principles calculations are conducted to reveal the behavior of a coating layer on an active material particle by focusing on the intercalation energy variation, lithium-ion transport, electron chemical potential change, and structural changes of the coating layer. The analysis comprehensively explains an experimental observation that a CeO_2 coating on $LiMn_2O_4$ particles exhibits better performance in capacity and cycling than an Al_2O_3 coating on the same particles. The fundamental knowledge imparted from this work provides an important understanding about the beneficial role of ALD coatings in lithium-ion battery performance and capacity retention.

1. Introduction

The current performance of battery technology cannot satisfy the increasing demand for long-lasting and efficient energy storage for future high energy and power applications. Higher energy and power density, robust cycling performance, and enhanced safety for lithium-ion batteries (LIBs) are the persistent needs that must be met in order to achieve increased functionality and versatility of consumer electronics [1]. Several families of active materials that serve LIB electrodes (anode and cathode) have attracted attention as possible materials for the next generation of high-performance LIBs. However, all electrode materials for LIBs suffer from degradation phenomena, including solid electrolyte interphase (SEI) layer formation, stress-induced degradation, mechanical fracture, and transition metal dissolution of the active material [2–5]. For anodes, the SEI layer initially serves as a protective layer formed on the active particle surface but becomes unstable over numerous cycles, which exacerbates the aging of cells. Furthermore, the developed stress due to volume change during Li ion intercalation causes mechanical fracture of the electrode and any attached layers, accelerating capacity loss. For cathodes, one key challenge is the dissolution of transition metal ions that becomes expedited at elevated temperatures. During the dissolution of transition metal ions, the structure of transition metal-based cathodes undergoes morphological changes, which in turn reduces the number of the available positions for Li ion intercalation. Additionally, some metals (e.g., Mn^{4+}), which have higher oxidation ability, can cause the decomposition of electrolyte solvents producing deleterious effects on battery performance. Fortunately, several approaches exist that can arrest these degradation processes. In particular, interface engineering by coating technology is an effective solution, as cell aging in both cycling and storage is rooted primarily from the side reactions at the electrode–electrolyte interfaces [6–8].

To date, the coating materials investigated in LIB applications include diverse carbon species and structures, metal oxides (e.g., Al_2O_3, ZrO_2, ZnO, and SiO_2) [9–11], and metal phosphates (e.g., $AlPO_4$) [12–13]. Most of the coating fabrication strategies have been based on sol–gel methods [14–15]. However, sol–gel methods typically cannot achieve uniformly thin, defect-free coatings and are beset by defects such as pinholes as well as high layer thickness, resulting in unstable interfaces that lead to poor performance and short cycle life [16]. To achieve a significant performance improvement, an ultrathin, conformal film coating is needed. Atomic layer deposition (ALD) is an efficient approach to create such ultrathin films, in which strong chemical bonds

* Corresponding author.
E-mail address: parkjonghy@mst.edu (J. Park).

https://doi.org/10.1016/j.cej.2022.135565
Received 10 December 2021; Received in revised form 2 February 2022; Accepted 27 February 2022
Available online 3 March 2022

are created to maintain the physical integrity between the substrate and the coating layer to produce sub-micron thick coatings. Recently, ultrathin film coatings have achieved significant performance improvements and have been implemented on active material surfaces, including $LiNiO_2$ [17], $LiCoO_2$ [18–20], $Li[Li_{0.20}Mn_{0.54}Ni_{0.13}Co_{0.13}]O_2$ [21], and Fe_3O_4-reduced Graphene Oxide [22]. The Li_3PO_4 coatings [23–26] have been demonstrated to significantly improve cell performance. Li-excessed $LiNiO_2$, $LiCoO_2$, and $LiMn_2O_4$ [27–28] active materials have exhibited better performance when coated with an Al_2O_3 ALD ultrathin film. In particular, an ultrathin CeO_2 film coating on LMO has significantly improved capacity and cycling performance compared to uncoated samples as well as Al_2O_3-coated samples at room and high temperatures [29–30]. While numerous experiments have been done to obtain cycling improvement and optimized performance via ALD coatings, few works have been conducted to understand the mechanistic role of an ALD coating in enhancing battery performance.

Among the few works that have been conducted to understand how an ALD coating can realize performance improvement, researchers have focused on providing guidance for high-performance LIBs by identifying the reduced oxygen evolution and thermal stability of Al_2O_3-coated $LiNiO_2$ surface using first-principles calculation [17], where the thermodynamic and kinetic properties of surface coatings play a vital role in the electrochemical performance of LIBs. To identify the behavior of Li ion transport in crystalline and amorphous coatings, Density Functional Theory (DFT) calculations and statistical mechanics have been combined. It was concluded that Li ions have slower diffusion in crystalline α-AlF_3, α-Al_2O_3, m-ZrO_2, and c-MgO coating due to a larger migration barrier (>0.9 V) that must be overcome. However, amorphous Al_2O_3 (am-Al_2O_3) and amorphous AlF_3 (am-AlF_3) showed smaller Li ion migration barriers and, thus, had significantly faster diffusion than the crystalline structure [31]. Investigation into the Li ion diffusivity in Lithium Lanthanum Titanium Oxides (LLTO) [32], Li_2NiO_2 and Li_xCoO_2 structures indicated that the activation barrier was very sensitive to the lithium concentration [33–34]. Moreover, different Li ion diffusion characteristics and behaviors in Al_2O_3 coating on LMO and SiO_2 coating on Si have been observed with different Li ion concentrations [35–40]. While these works revealed that the structure and composition of the coating layer influenced Li intercalation and diffusivity, these studies limited their investigation to the coating layer without consideration of the influence of the adjacent active materials, limiting the understanding of the coating and active material interactions and behavior.

In particular, the phenomenon at the interface between the active material and coating layer is not well understood as most previous works focused only on the coating layer itself. As Li ions must intercalate from the coating layer to the active material, the surrounding coating environment can influence the behavior of Li ion intercalation into active materials. Without consideration of the adjacent active material, a large gap remains in understanding the behavior of Li mobility from the coating to the active particle. As Li ions must first travel through the coating layer to reach the active material, the composition of the coating layer may impact Li diffusivity, thus the ionic transport through the coating layer must be understood. Furthermore, as Li ions pass through the coating layer, a volume change can occur and cause mechanical failure after repeated cycles, making it necessary to comprehend the mechanical property of different coatings. The objective of the present work is to seek answers to these questions and to clarify our previous experimental observation [29]: an electrode made of CeO_2-coated $LiMn_2O_4$ (LMO) particles showed improved performance over an electrode made of Al_2O_3-coated LMO particles. In the previous work, it was demonstrated that a CeO_2 coating layer could provide higher performance and stability over uncoated active particles and other coating materials, such as Al_2O_3. Although a faster lithium ion transport was identified in the CeO_2 coating layer compared to the Al_2O_3 coating layer [29], the interfacial physics between coating and active material is still unknown. Therefore, in this work, CeO_2 and Al_2O_3 coatings on $LiMn_2O_4$ cathode particles were studied and different parametric aspects of the coating were analyzed based on first-principles calculations, including thermodynamic preferences, ionic transport, and structural changes.

2. Computational method

The Li ion transport in ultrathin coatings can be explained by several different physical aspects. From the thermodynamic aspect, the energy relevant to intercalation can be different depending on the coating material and the concentration of lithium ions. Formation energy calculation is an energetic point of evaluation and is one of the most common approaches to analyze the Li ion intercalation behavior [31,35,41–48], and was thus calculated and studied. By comparing the total energy change of Al_2O_3 and CeO_2-coated LMO before Li ion intercalation, after Li ion intercalation into the coating, and after Li ion intercalation into LMO particles, the preference of intercalation into the coating layer and active material can be determined. In particular, the active material impact on Li ion transportation has been considered, which was found to have a significant impact on the behavior. To reveal the interfacial reaction between active material and coating layer, Li ion intercalation preference indicated by the barrier energy of Li ion transportation of coated active materials as well as the resulting coating layer structural changes were investigated by first-principles calculation. LMO slab structures with (0 0 1), (1 1 0), and (1 1 1) surface orientation have been studied extensively [49] and showed that LMO with (0 0 1)_Li_2 surface orientation structure had the lowest surface energy and, thus, is the most stable surface orientation. Therefore, LMO with (0 0 1)_Li_2 slab structure was prioritized in this work. Density functional theory calculations and Ab initio molecular dynamics simulations were performed by using Vienna Ab initio Simulation Package (VASP) code [50–51]. The Perdew – Burke – Ernzerhof (PBE) exchange and correlation functional and the projector augmented wave (PAW) method were applied [52]. The electronic wave functions were expanded on a plane-wave basis set of 400 eV for $Li_xAl_2O_3$ and Li_xCeO_2 system, and 600 eV for Al_2O_3-coated $LiMn_2O_4$ and CeO_2-coated $LiMn_2O_4$ system, in which the Dudarev's rotationally invariant DFT + U functional was performed to treat the 3d electrons of Mn ions [53] and U values for Mn is 4.84 eV [54]. The amorphous $Li_xAl_2O_3$ structure contained 10 × x Li, 20 Al, and 30O, and the amorphous Li_xCeO_2 structure contained 10 × x Li, 10 Ce, and 20O in the cubic supercell. The amorphous structures were created by quench processing [36], which was performed by ab initio Molecular Dynamic (MD) simulation, where the initial random structure was heated from 300 K to 3000 K, followed by an equilibration process for 1 ps, and finally cooling from 3000 K to 300 K. Varying Li ion concentrations in $Li_xAl_2O_3$ and Li_xCeO_2 ($0 \leq \times \leq 1$) were considered to study the formation energy, volume expansion, and structural evolution, where a broad range of the lithiation state in those coating materials was analyzed. The electrochemical kinetics of a cell can be represented by the following three key steps: (1) Li conduction through the electrolyte and insertion into the active particle, (2) electron conduction and insertion into the active particle, and (3) Li diffusion through the active particle. As active materials are typically mixed ion and electron conductors, either the ionic or electronic transport may be the kinetically limiting step for the electrochemical reactions depending on the degree of ionic and electronic conductivity of the active material [55]. Since most electrode materials have a degree of electronic conductivity that is often larger than its Li ion conductivity, it is reasonable to consider ionic mobility as the limiting factor [56–57]. Therefore, the formation energy of $Li_xAl_2O_3$ and Li_xCeO_2 as a function of Li ion concentration was calculated and compared. The formation energy [35,58] of $Li_xAl_2O_3$ and Li_xCeO_2 was defined as follows:.

$$E_{f(x)} = E_{tot}(Li_xAl_2O_3 or Li_xCeO_2) - xE_{tot}(Li) - E_{tot}(Al_2O_3 or CeO_2) \quad (1)$$

where E_{tot} $(Li_xAl_2O_3)$ and E_{tot} (Li_xCeO_2) are the total energy per $Li_xAl_2O_3$ unit and per Li_xCeO_2 unit, respectively, E_{tot} (Li) is the total energy per atom of bcc Li bulk, and E_{tot} (Al_2O_3) and E_{tot} (CeO_2) are the total energy

per Al_2O_3 unit and per CeO_2 unit, respectively.

From the kinetic aspect, the Li ion concentration impact on Li ion intercalation into LMO from the amorphous coating was studied. For this, the barrier energy was calculated during Li ion transportation by performing the CINEB (climbing nudged elastic band) method [31,33–34,59–60] on various diffusion paths, in which three images between the initial configuration and final configuration were selected to calculate the Li ion transportation barrier energy. In general, the NEB method has been used for both crystalline and amorphous materials [61–63]. Furthermore, ab initio MD simulation was used to calculate the Li ion diffusivity through the Al_2O_3 and CeO_2 coating layer, itself. The atomic structures for these studies are shown in Fig. 2. The system size of $Li_xAl_2O_3$ and Li_xCeO_2 was determined by a convergence test and the final number of atoms, the termination, and the orientation were selected as follows: Al_2O_3 (12Al, 18O) and CeO_2 (7Ce, 14O) coated $LiMn_2O_4$ (16Li, 32Mn and 64O) structure [49] with Li-terminated (0 0 1) surface orientation (001_Li_2). To calculate Li ion diffusivity in $Li_xAl_2O_3$ and Li_xCeO_2 as a function of Li ion concentration, the Nosé-Hoover thermostat [35,58,64–68] was used to control the temperature, and ab initio MD simulations were performed at T = 1200 K, 1600 K, 2000 K, and 2400 K, respectively. Then, the Li diffusion coefficient $D_{@1200K}$, $D_{@1600K}$, $D_{@2000K}$, and $D_{@2400K}$ can be calculated based on the Einstein relation [35]:.

$$< r^2(t) >= 6Dt \tag{2}$$

where $< r^2(t) >$ is the mean square displacement of Li, D is the Li diffusion coefficient, and t is time. The Li diffusion coefficients at 1200 K, 1600 K, 2000 K, and 2400 K were used to extrapolate the Li diffusion coefficient at $T = 300$ K based on the Arrhenius law

$$D = D_0 \exp(-E_D/k_B T) \tag{3}$$

where D_0 is the pre-exponential factor, E_D is the barrier energy for diffusion, T is temperature, and k_B is the Boltzmann constant. The D_0 and E_D values can be obtained from four points (1200 K, $D_{@1200K}$), (1600 K, $D_{@1600K}$), (2000 K, $D_{@2000K}$), and (2400 K, $D_{@2400K}$). Then, the Li diffusion coefficient at 300 K ($D_{@300K}$) can be calculated based on the Arrhenius law.

Lastly, from the mechanical aspect, during the intercalation of Li, there is a volume change that is associated with the mechanical damage of the coating itself. Therefore, the volume expansion was calculated as a function of the coating thickness. From the atomistic and electronic structural aspect, the radial distribution function and the charge state of atoms were calculated to investigate the structure evolution of amorphous $Li_xAl_2O_3$ and Li_xCeO_2. For the volume expansion calculation, both the shape and volume were allowed to change with a 3 × 3 × 3 Monkhorst-Pack mesh [35,69] and 520 eV cutoff energy [35,37,58].

3. Results

The first step in the intercalation of Li ions into the coated active material is the introduction of Li ions into the coating layer. To understand this first step, the formation energy of $Li_xAl_2O_3$ and Li_xCeO_2 as a function of Li ion concentration was calculated and compared. As shown in Fig. 1, the negative formation energies indicate that Li intercalation into the coating materials is preferred, and the formation energy of $Li_xAl_2O_3$ ($0 \leq \times \leq 1$) agreed well with the reported value [35]. The formation energy for Li_xCeO_2 was much lower for all Li ion concentrations, which suggested Li ion could intercalate into the CeO_2 coating layer more easily than in the Al_2O_3 coating layer.

In a previous study [35] based on the formation energy calculation, Li ions preferred to stay in the coating layer as long as the formation energy was lower. However, this is only the case when a coating layer is isolated from an active material. In reality, after Li ions pass through the coating, the Li ions must eventually intercalate into the active materials to complete the redox reactions. As the coating layer may change the Li ion intercalation behavior of the active material, it is necessary to consider the active material along with the coating layer to capture the actual physics. To study this, a 0.5 nm thick CeO_2 coating layer was placed on top of the LMO active material. Then, the energies from three different stages of the intercalation process into the active material were compared: (I) before intercalation (Li ions outside of the coating layer), (II) Li ions residing in the coating layer, and (III) Li ions intercalation into the active material.

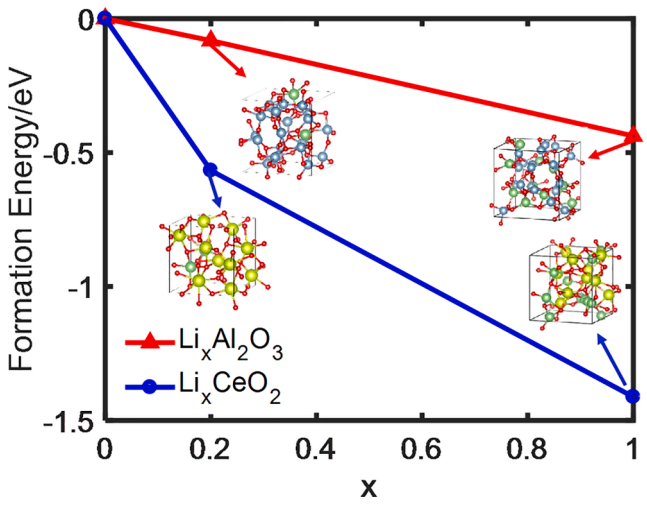

Fig. 1. Formation energy of $Li_xAl_2O_3$ and Li_xCeO_2 as a function of lithium content without active material.

From the stage (I) to stage (II), to examine whether Li ions preferred to intercalate into the coating material, the total energy changes before and after the intercalation into the Al_2O_3 and CeO_2 coating layers were calculated and were found to be −5.71 eV and −3.42 eV, respectively (Table 1). This implied that Li ions favored intercalation into both coating layers. Here it can be noted that Al_2O_3/LMO showed a lower energy than the case of CeO_2/LMO for the initial intercalation into the coating layer. Next, to see whether Li ions further favored intercalation into the active material from the coating layers, the total energy change before and after the intercalation into LMO was calculated, where the energy changes were 2.53 eV and 1.59 eV for Al_2O_3 and CeO_2, respectively. By comparison to the initial intercalation into the coating, the Li ion in the coatings tended to stay in the coating layer rather than intercalate into the active material for both the Al_2O_3 and CeO_2 coating layers. This was different from the description of the previous case (Fig. 1), which was without any consideration of active material impacts.

However, if Li ions prefer to stay in the layer, no intercalation into the active particle can happen, which is not true. We then examine another possibility, that is as one more Li ion comes into the layer, the interaction among atoms (intercalated Li ions and coating layer host atoms) changes the environment, thus impacting Li ion intercalation behavior. To examine this, two Li ions' intercalation processes have been tested. As listed in Table 2, the final stage with two Li ions intercalated into the active material showed the lowest energy level for both coating materials. The energy change for each step was −9.89 eV and

Table 1
Energy change during one Li ion intercalation[a].

structure	$E_{coating}$ (eV)	E_{LMO} (eV)
Al_2O_3/LMO	−5.71	2.53
CeO_2/LMO	−3.42	1.59

([a] Energy change before Li ion intercalation, one Li ion intercalation into the coating, and one Li ion intercalation into LMO. $E_{coating}$ is the energy change after one Li ion intercalation into the coating, and E_{LMO} is the energy change after one Li ion intercalation into the LMO particle.).

Table 2
Energy change during two Li ion intercalation[a].

Structure	$E_{coating}$ (eV)	E_{LMO} (eV)
Al_2O_3/LMO	−9.89	−2.02
CeO_2/LMO	−2.58	−2.98

([a] Energy change before two Li ions intercalation, two Li ions intercalation into the coating and two Li ions intercalation into the LMO particle. $E_{coating}$ is the energy change after one Li ion intercalation into the coating, and E_{LMO} is the energy change after one Li ion intercalation into the LMO particle.).

−2.02 eV for the Al_2O_3 coating layer, and −2.58 eV and −2.98 eV for the CeO_2 coating layer. These results implied that unlike one Li ion, two Li ions would further intercalate into the active material after intercalating into the coating layer. Also, a CeO_2 layer showed a lower energy level for the intercalation into the active material when compared to Al_2O_3, which can be thermodynamic evidence of the observed improved performance of CeO_2 coating over the Al_2O_3 coating [29]. Here, in our atomic structures, the stoichiometric values are 0.14 and 0.29 in Li_xCeO_2, with × corresponding to one and two Li ions, respectively, and the $Li_xAl_2O_3$ stoichiometric values are 0.17 and 0.33, with × corresponding to one and two Li ions, respectively. The energy change of $Li_xAl_2O_3$/LMO and Li_xCeO_2/LMO during Li ion intercalation into LMO at different Li ion concentrations was then considered. As shown in Fig. 2 and Table A2, we found that the energy change of $Li_xAl_2O_3$/LMO reached the minimum when × = 0.5, while the energy change of Li_xCeO_2/LMO reached the minimum when × = 0.29. This indicates that the intercalated Li ions into the coating layer may stay until there is a sufficient accumulation of ions that can then move the intercalated Li ions further into the active material. An accumulation of ions then causes more volume expansion in Al_2O_3 coating than that in CeO_2 coating. Thus, there will be more mechanical damage incurred in the Al_2O_3 coating than in the CeO_2 coating. For this possible scenario, there is an experimental evidence that the coating thickness undergoes volume change during the intercalation process [28]. Our result could be an indirect support of this reported finding, where the Li ions entering into the coating layer may accumulate due to the energy barrier to the intercalation into the active material, and the accumulated Li ions can then induce a limited volume change before intercalation into the active material.

To examine how Li ions transport from the coating to the active material (stage (II) to stage (III)), the barrier energy of Li ion intercalation to the active material from the coating layer was calculated by using the CINEB method. Several Li ions diffusion pathways were considered, and the lowest barrier energy of Li ion diffusion pathway is shown in Fig. 3. The Li ion barrier energy of Al_2O_3-coated LMO was 2.64 eV and barrier energy for CeO_2-coated LMO was 2.02 eV. This energy barrier prevented the intercalated Li ions from passing through the coating layer to move into the active material, as described above. Furthermore, the barrier energy for the CeO_2 coating was lower than that for the Al_2O_3 coating, meaning that it was easier for Li ions to intercalate into the active material with the CeO_2 layer.

To identify the electron transfer capability of the $Li_xAl_2O_3$/LMO and Li_xCeO_2/LMO when Li ions intercalate from coating to the LMO active material, the electron chemical potential difference of $Li_xAl_2O_3$/LMO and Li_xCeO_2/LMO during Li ion intercalation from the coating into the LMO active material were calculated. Basically, the Fermi energy difference (ΔF) equals the electron chemical potential difference (Δu) in the same system [70–71]. As shown in Table 3, it was found that the Fermi energy of Li ions in the Al_2O_3 coating and LMO were 0.51 eV and −0.08 eV respectively. The electron chemical potential difference was 0.59 eV, which indicated the $Li_xAl_2O_3$ coating tended to transfer electrons to LMO active material. Meanwhile, the electron chemical potential of Li ions in the CeO_2 coating and LMO were 3.55 eV and 0.05 eV, respectively. This meant that the electron chemical potential difference of CeO_2/LMO was much higher than that of Al_2O_3/LMO, which indicated that the CeO_2/LMO interface was more likely to transfer electrons to LMO active material than the Al_2O_3/LMO interface.

As Li ions should diffuse through the coating layer first, another important property of coating material influencing battery performance is the Li ion diffusivity. To investigate the transport property of $LiAl_2O_3$ and $LiCeO_2$ coating, the mean square displacement $< r^2 (t) >$ of Li ions was calculated by performing ab initio MD simulation at 1200, 1600, 2000, and 2400 K. The $D_{@1200K}$, $D_{@1600K}$, $D_{@2000K}$, and $D_{@2400K}$ was calculated based on the Einstein relation (Figures A2 and Figures A3). Then, according to the Arrhenius law, the pre-exponential factor (D_0), the barrier energy for diffusion (E_D), and Li ion diffusivity at 300 K ($D_{@300K}$) can be obtained [35]. As shown in Table 4, the diffusion coefficient of $LiCeO_2$ at 300 K was higher than that of $LiAl_2O_3$, which could be another piece of evidence to explain the observed better battery performance found in the CeO_2 coated particles compared to that of the Al_2O_3 coated particles.

One important concern is the mechanical damage of the coating layer itself due to the volume changes during intercalation and deintercalation of Li ions. To study the mechanical behavior of coating materials during lithiation, the volume expansion of $Li_xAl_2O_3$ and Li_xCeO_2 was calculated. As shown in Fig. 4, the volume expansion of $Li_xAl_2O_3$ and Li_xCeO_2 increased with increasing Li ion concentration. The

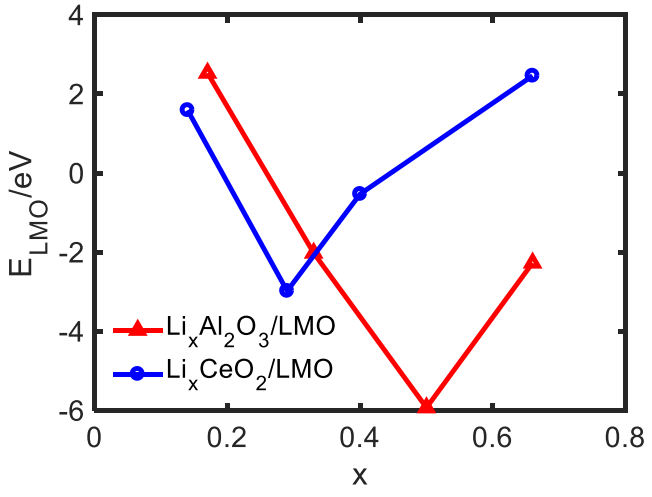

Fig. 2. Energy change of $Li_xAl_2O_3$ /LMO and Li_xCeO_2 /LMO during Li ion intercalation into LMO at different Li ion concentrations.

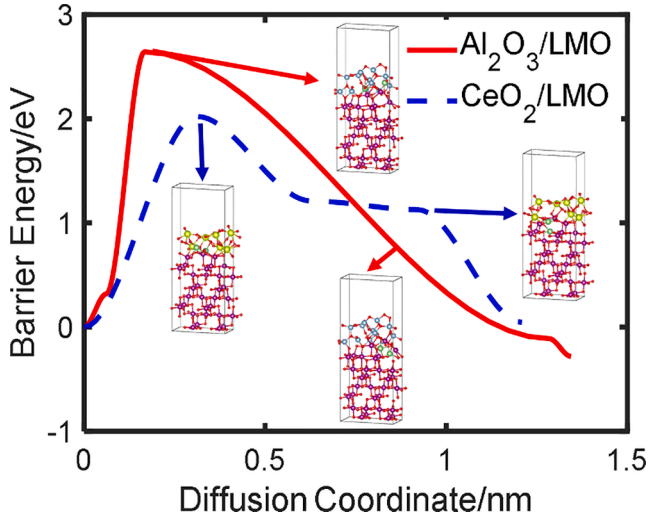

Fig. 3. Barrier energy of Al_2O_3 and CeO_2-coated $LiMn_2O_4$ with intercalation of two Li ions.

Table 3
Fermi energy during two Li ion intercalation.

Structure	$Fermi_{coating}$ (eV)	$Fermi_{LMO}$ (eV)	ΔF/Δu(eV)
Al_2O_3/LMO	0.51	−0.08	0.59
CeO_2/LMO	3.55	0.05	3.50

Table 4
Li ion diffusion coefficients of $LiAl_2O_3$ and $LiCeO_2$ at 300 K.

Structure	$D_{@300K}$ (cm^2/s)
$LiAl_2O_3$	1.81E-11
$LiCeO_2$	4.15E-09

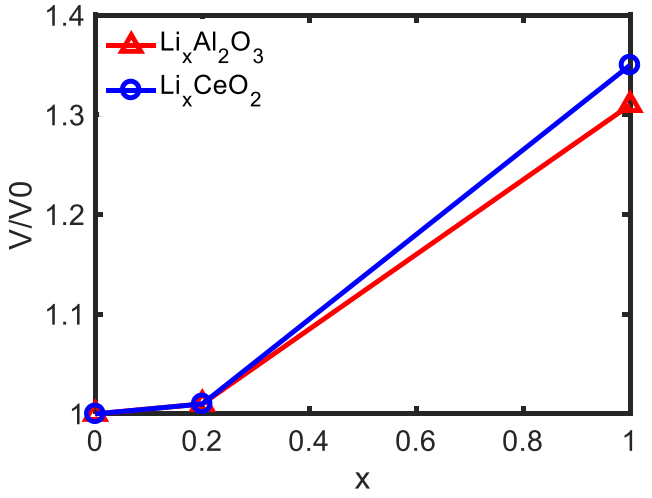

Fig. 4. Comparison of the volume expansion of $Li_xAl_2O_3$ and Li_xCeO_2 without active material.

volume expansion was determined by the Li:Al and Li:Ce ratio of the coating; the result shows that the volume expansion was very similar between the two coating materials when x = 0.2, where the Li:Al and Li:Ce ratios were 0.1 and 0.2, respectively, indicating that the same amount of Li ions would produce a lower volume expansion in the CeO_2 coating. As discussed earlier, Li ions always tended to intercalate into LMO particles after passing through the coating. When comparing the two coating materials, Al_2O_3 showed a higher volume expansion, which could lead to a higher possibility of damage of the coating layer and could also explain why the CeO_2 coating produced better LIB performance.

To obtain insight into the physical changes occurring during intercalation, further detailed structural changes of the coating materials were studied by ab initio MD simulations. First, through analyzing the radial distribution function (RDF), it was found that the Li-O bond length of $Li_xAl_2O_3$ (Fig. 5A) and Li_xCeO_2 (Fig. 5D) was about 2.0 Å, which agreed well with the experimental data of 1.9 Å of Li_2O_2 [35,72]. The Li–O bond length of 2.0 Å and Al − O bond length of 1.8 Å and Ce–O bond length of 2.2 Å remained unchanged with increasing Li ions (Fig. 5A, B, D, and E). The Al–O bond length of 1.8 Å was the same as the reported value [35], and the Ce − O bond length of 2.2 Å agreed well with the reported Ce–O bond length of 2.15 Å [73]. However, the Al − Al and Ce–Ce bond length kept changing during lithiation. At low Li ion concentration, the Al − Al bond length was 3.2 Å and the Ce − Ce bond length was 3.8 Å (Fig. 5F). The Ce − Ce bond length was 3.8 Å (Fig. 5F) at concentration × = 0, which agreed with the reported Ce–Ce bond length of 3.826 Å of cubic CeO_2 [74]. As Li ion concentration increased, the Al-Al bond length decreased from 3.2 Å (x = 0) to 2.8 Å (x = 0) (Fig. 5C) and Ce-Ce bond length peak changed from 3.8 Å (x = 0) to 3.6 Å (x = 1) (Fig. 5F), indicating that individual Al and Ce atoms had a variety of charge states during lithiation. Furthermore, the Bader charge analysis was then used to quantify the charge distribution of atoms in $Li_xAl_2O_3$ and Li_xCeO_2 coating during lithiation, where the charge analysis can reflect the amorphous structure alternation. During lithiation, the charge state of Al changed from + 2.5 (x = 0) to + 2.0 (x = 1) and Ce had a change from + 2.2 (x = 0) to + 1.9 (x = 1) (Fig. 6A and 6B). This suggested that individual Al and Ce had various charge states during lithiation, which was consistent with RDF results. The various charge

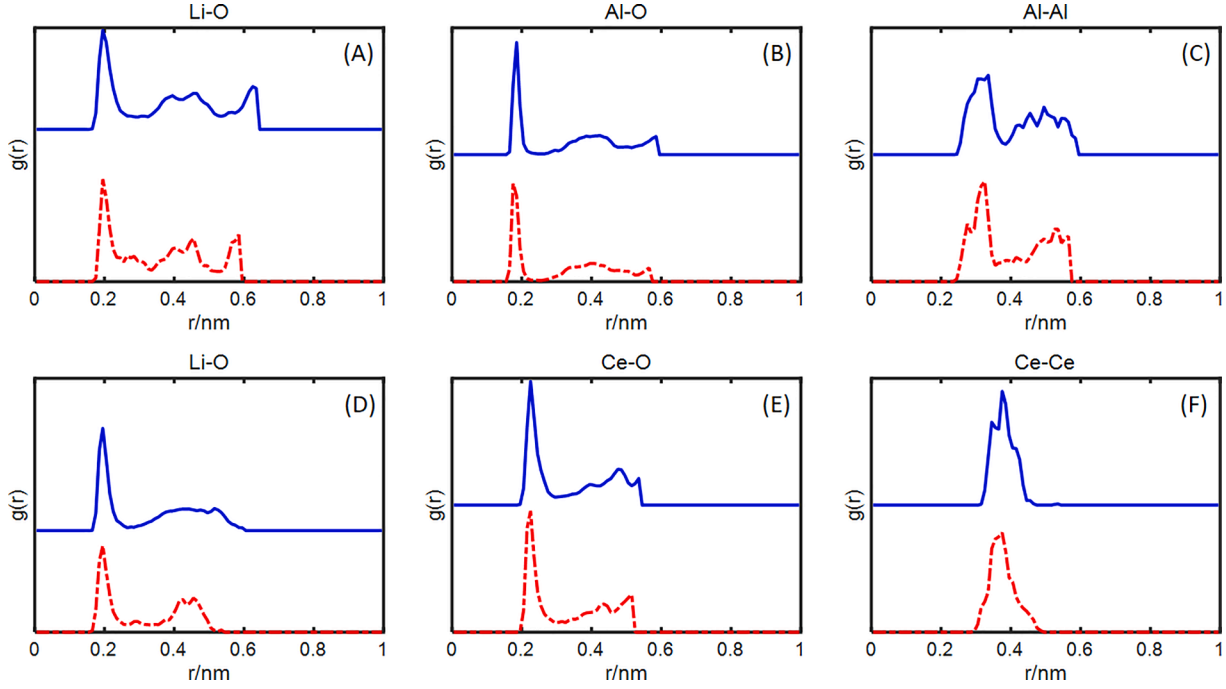

Fig. 5. Radial distribution function of (A) Li-O, (B) Al-O, (C) Al-Al in $Li_xAl_2O_3$ and (D) Li-O, (E) Ce-O, (F) Ce-Ce in Li_xCeO_2(red dot line: x = 0.2; blue line: x = 1).

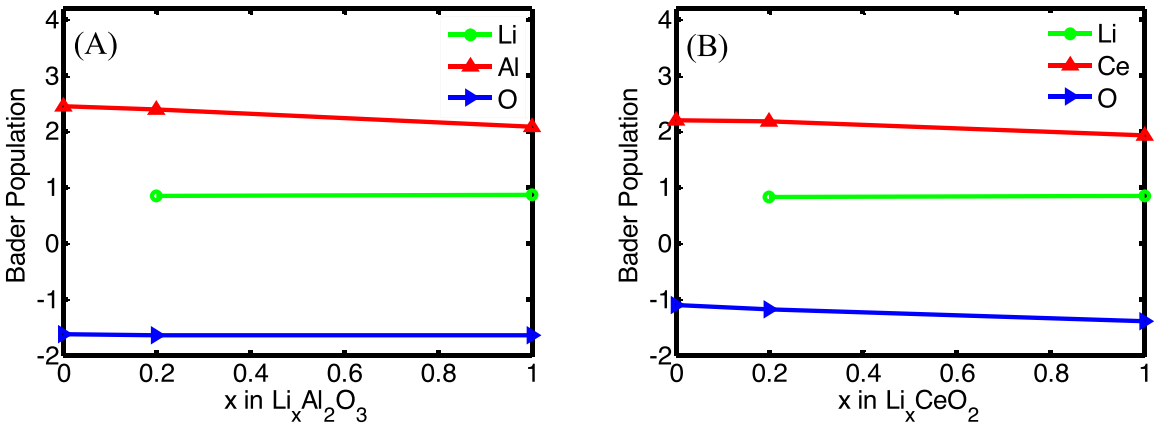

Fig. 6. Bader population of (A) $Li_xAl_2O_3$ and (B) Li_xCeO_2.

states of Al and Ce mainly originated from the incoming Li and indicated that different Al and Ce bonding state existed coincidentally, thus proving that there existed isolated Al and Ce atoms and atomic clusters inside $Li_xAl_2O_3$ and Li_xCeO_2 coating during Li ion intercalation. Meanwhile, the charge state of Li in $Li_xAl_2O_3$ and Li_xCeO_2 were very close to + 1 during Li diffusion inside coating. The charge state of O was relatively constant over the entire range of Li concentrations in $Li_xAl_2O_3$, and the charge state of O in the Li_xCeO_2 not only varied more than $Li_xAl_2O_3$ but also was less negative for most of the Li concentration range. The relatively low negative charge state of O in Li_xCeO_2 produced a weaker interaction between passing Li and O in the structure compared to a high negative charge state of O, which tended to hold the positively charged Li more strongly. Thus, the low negative charge state of O can not only accelerate Li transport through coating but also reduce Li diffusion barrier on the coating/cathode interface when Li intercalate into active materials, which could also explain why Li_xCeO_2 coating shows better performance than Al_2O_3 coating in LIBs.

4. Conclusions

In this work, a study was conducted on the thermodynamic preference, ionic transport, and structural changes of Al_2O_3 and CeO_2 coatings on $LiMn_2O_4$ cathode particles, elucidating the mechanism behind the improved performance of CeO_2-coated active material over that of Al_2O_3-coated active material through first-principles calculations. First, from the calculated formation energy for Li intercalation into the coating layer itself, the energy level of Li_xCeO_2 was lower than that of $Li_xAl_2O_3$, indicating that Li ions can more effortlessly intercalate into a CeO_2 coating than in an Al_2O_3 coating. Meanwhile, the Fermi energy change of CeO_2/LMO during Li ion intercalation is higher than Al_2O_3/LMO, indicating the CeO_2/LMO is more likely to transfer electrons to LMO active material. Next, considering the $LiMn_2O_4$ active material along with Al_2O_3 and CeO_2 coating layers, the energy change during Li ion intercalation was calculated to find that, when compared to one Li ion, two Li ions could further intercalate $LiMn_2O_4$ after passing through Al_2O_3 and CeO_2 coatings. However, there is a barrier energy that must be overcome. Our finding shows that barrier energy of Li ion transportation from CeO_2 coating to active material is lower than that of Al_2O_3 coating, suggesting easy intercalation of Li ions in $LiMn_2O_4$ from a CeO_2 coating than from a Al_2O_3 coating. Kinetically, Li ions in $LiCeO_2$ coating diffuse faster than those in $LiAl_2O_3$ coating, which could explain the observed improved performance of CeO_2 coating reported in our previous work. From the structural change analysis, we found that charge state of Al and Ce atoms have a huge variation during Li ions intercalation and that the negative charge state of O atoms in Li_xCeO_2 coating was lower than that in $Li_xAl_2O_3$, which produces a weaker interaction between the passing positive charge Li atoms and negative charge O atoms and explain the higher Li diffusivity in Li_xCeO_2 coating during Li ion intercalation. In summary, this work provides a clear understanding of the behavior of ALD coatings with active materials and how the ALD coating is beneficial to LIB, giving evidence as to why a CeO_2 ALD coating has improved performance than other binary coating material during the lithiation process from the fundamental study at the electronic level.

Declaration of Competing Interest

The authors declare that they have no known competing financial interests or personal relationships that could have appeared to influence the work reported in this paper.

Acknowledgments

The authors gratefully acknowledge financial support from the National Science Foundation (CBET 1510085 and CMMI 1917055).

Appendix A. Supplementary data

Supplementary data to this article can be found online at https://doi.org/10.1016/j.cej.2022.135565.

REFERENCES

[1] A. Manthiram, Y. Fu, S.H. Chung, C. Zu, Y.S. Su, Rechargeable Lithium-Sulfur Batteries, Chemical Reviews 114 (23) (2014) 11751–11787.
[2] P. Verma, P. Maire, P. Novák, A review of the features and analyses of the solid electrolyte interphase in Li-ion batteries, Electrochimica Acta 55 (22) (2010) 6332–6341.
[3] S. Sarkar, R.L. Patel, X. Liang, J. Park, Unveiling the role of ceo 2 atomic layer deposition coatings on limn 2 o 4 cathode materials: an experimental and theoretical study unveiling the role of ceo2 atomic layer deposition coatings on limn2o4 cathode materials: an experimental and theoretical study, *ACS applied materials & interfaces* 9 (36) (2017) 30599–30607.
[4] M. Ebner, F. Marone, M. Stampanoni, V. Wood, Visualization and quantification of electrochemical and mechanical degradation in Li ion batteries, Science 342 (6159) (2013) 716–720.
[5] V. Etacheri, R. Marom, R. Elazari, G. Salitra, D. Aurbach, Challenges in the development of advanced Li-ion batteries: a review, Energy & Environ. Sci. 4 (9) (2011) 3243–3262.
[6] J. Cabana, B.J. Kwon, L. Hu, Mechanisms of degradation and strategies for the stabilization of cathode-electrolyte interfaces in li-ion batteries, Accounts of Chem. Research 51 (2) (2018) 299–308.
[7] M. Gauthier, T.J. Carney, A. Grimaud, L. Giordano, N. Pour, H.-H. Chang, D. P. Fenning, S.F. Lux, O. Paschos, C. Bauer, F. Maglia, S. Lupart, P. Lamp, Y. Shao-Horn, Electrode–electrolyte interface in li-ion batteries: current understanding and new insights, J. Phys. Chem. Lett. 6 (22) (2015) 4653–4672.
[8] S.-J. Yang, W.-J. Song, D.B. Dingwell, J. He, H.-B. Guo, Surface roughness affects metastable non-wetting behavior of silicate melts on thermal barrier coatings, Rare Metals 41 (2) (2022) 469–481.
[9] J. Cho, Y. Kim, B. Park, Novel $LiCoO_2$ cathode material with Al_2O_3 Coating for a Li Ion Cell, Chem. Mater. 12 (2000).
[10] Y.-K. Sun Y. Lee s., Yoshio, M., Amine, K.,ELECTROCHEM SOLID STATE LETT, Synthesis and Electrochemical Properties of ZnO-Coated LiNi0.5Mn1.5O4 Spinel as

5 V Cathode Material for Lithium Secondary Batteries Electrochemical and Solid State Letters - 5 2002.
[11] Z. Chen, J. Dahn, Studies of $LiCoO_2$ Coated with Metal Oxides, Electrochemical and Solid-State Letters 6 (2003) A221.
[12] A.T. Appapillai, A.N. Mansour, J. Cho, Y. Shao-Horn, Microstructure of $LiCoO_2$ with and without "$AlPO_4$" nanoparticle coating: Combined STEM and XPS studies, Chemistry Of Materials 19 (23) (2007) 5748–5757.
[13] Y. Bai, N. Liu, J. Liu, Z. Wang, L. Chen, Coating material-induced acidic electrolyte improves $LiCoO_2$ performances, Electrochemical And Solid State Letters 9 (12) (2006) A552–A556.
[14] Y. Zhang, C.S. Sun, Z. Zhou, Sol-gel preparation and electrochemical performances of $LiFe_{1/3}Mn_{1/3}Co_{1/3}PO_4$/C composites with core-shell nanostructure, Electrochemistry Communications 11 (6) (2009) 1183–1186.
[15] Y.-K. Sun, S.-T. Myung, B.-C. Park, J. Prakash, I. Belharouak, K. Amine, High-energy cathode material for long-life and safe lithium batteries, Nature Materials 8 (4) (2009) 320–324.
[16] Z. Chen, Y. Qin, K. Amine, Y.K. Sun, Role of surface coating on cathode materials for lithium-ion batteries, J. Mater. Chem. 20 (36) (2010) 7606–7612.
[17] J. Kang, B. Han, First-principles study on the thermal stability of $linio_2$ materials coated by amorphous al_2o_3 with atomic layer thickness, ACS Applied Materials & Interfaces 7 (21) (2015) 11599–11603.
[18] Y.S. Jung, A.S. Cavanagh, L.A. Riley, S.-H. Kang, A.C. Dillon, M.D. Groner, S. M. George, S.-H. Lee, Ultrathin direct atomic layer deposition on composite electrodes for highly durable and safe li-ion batteries, Adv. Materi. 22 (19) (2010) 2172–2176.
[19] J.-T. Lee, F.-M. Wang, C.-S. Cheng, C.-C. Li, C.-H. Lin, Low-temperature atomic layer deposited Al_2O_3 thin film on layer structure cathode for enhanced cycleability in lithium-ion batteries, Electrochimica Acta 55 (12) (2010) 4002–4006.
[20] J.H. Woo, J.E. Trevey, A.S. Cavanagh, Y.S. Choi, S.C. Kim, S.M. George, K.H. Oh, S.-H. Lee, Nanoscale interface modification of $LiCoO_2$ by Al_2O_3 Atomic Layer deposition for solid-state li batteries, J. Electrochem. Soc. 159 (7) (2012) A1120–A1124.
[21] Y.S. Jung, A.S. Cavanagh, Y. Yan, S.M. George, A. Manthiram, Effects of atomic layer deposition of Al_2O_3 on the $Li[Li_{0.20}Mn_{0.54}Ni_{0.13}Co_{0.13}]O_2$ Cathode for lithium-ion batteries, J. Electrochem. Society 158 (12) (2011) A1298–A1302.
[22] Q.-H. Wu, B. Qu, J. Tang, C. Wang, D. Wang, Y. Li, J.-G. Ren, An alumina-coated fe_3o_4-reduced graphene oxide composite electrode as a stable anode for lithium-ion battery, Electrochimica Acta 156 (2015) 147–153.
[23] X. Li, R. Yang, B. Cheng, Q. Hao, H. Xu, J. Yang, Y. Qian, Enhanced electrochemical properties of nano-Li_3PO_4 coated on the LiMn2O4 cathode material for lithium ion battery at 55 degrees C, Materials letters 66 (1) (2012) 168–171.
[24] X. Bian, Q. Fu, X. Bie, P. Yang, H. Qiu, Q. Pang, G. Chen, F. Du, Y. Wei, Improved electrochemical performance and thermal stability of li-excess $Li_{1.18}Co_{0.15}Ni_{0.15}Mn_{0.52}O_2$ Cathode Material by Li_3PO_4 Surface Coating, Electrochimica Acta 174 (2015) 875–884.
[25] D.R. Chen, F. Zheng, L. Li, M. Chen, X.X. Zhong, W.S. Li, L. Lu, Effect of Li_3PO_4 coating of layered lithium -rich oxide on electrochemical performance, Journal Of Power Sources 341 (2017) 147–155.
[26] J. Chong, S.D. Xun, J.P. Zhang, X.Y. Song, H.M. Xie, V. Battaglia, R.S. Wang, Li_3PO_4-Coated $LiNi_{0.5}Mn_{1.5}O_4$: A stable high-voltage cathode material for lithium-ion batteries, Chemistry-a European Journal 20 (24) (2014) 7479–7485.
[27] X. Zhang, I. Belharouak, L.i. Li, Y.u. Lei, J.W. Elam, A. Nie, X. Chen, R.S. Yassar, R. L. Axelbaum, Structural and electrochemical study of Al2O3 and TiO2 Coated Li1.2Ni0.13Mn0.54Co 0.13O2 cathode material using ALD, Adv. Energy Mater. 3 (10) (2013) 1299–1307.
[28] Y. Liu, N.S. Hudak, D.L. Huber, S.J. Limmer, J.P. Sullivan, J.Y. Huang, In situ transmission electron microscopy observation of pulverization of aluminum nanowires and evolution of the thin surface al_2o_3 layers during lithiation-delithiation cycles, Nano Letters 11 (10) (2011) 4188–4194.
[29] R.L. Patel, H. Xie, J. Park, H.Y. Asl, A. Choudhury, X. Liang, Significant capacity and cycle-life improvement of lithium-ion batteries through ultrathin conductive film stabilized cathode particles, Adv. Mater. Interfaces 3 (13) (2016).
[30] Y. He, H. Pham, Y. Gao, R.L. Patel, S. Sarkar, X. Liang, J. Park, Discovery of an unexpected metal dissolution of thin-coated cathode particles and its theoretical explanation, Adv. Theory and simulations 3 (5) (2020) 2000002.
[31] S. Xu, R.M. Jacobs, H.M. Nguyen, S. Hao, M. Mahanthappa, C. Wolverton, D. Morgan, Lithium transport through lithium-ion battery cathode coatings, J. Mater. Chem. A 3 (33) (2015) 17248–17272.
[32] D. Qian, B. Xu, H.-M. Cho, T. Hatsukade, K.J. Carroll, Y.S. Meng, Lithium Lanthanum Titanium Oxides: A Fast Ionic Conductive Coating for Lithium-Ion Battery Cathodes, Chem. Mater. 24 (14) (2012) 2744–2751.
[33] K. Kang, D. Morgan, G. Ceder, First principles study of Li diffusion in I-Li_2NiO_2 structure, Phys. Review B 79 (1) (2009), 014305.
[34] A. Van der Ven, G. Ceder, Lithium diffusion mechanisms in layered intercalation compounds, J. Power Sources 97–8 (2001) 529–531.
[35] S.C. Jung, Y.-K. Han, How do li atoms pass through the al_2o_3 coating layer during lithiation in li-ion batteries? J. Phys. Chem. Letters 4 (16) (2013) 2681–2685.
[36] S.C. Jung, Y.-K. Han, Ab initio molecular dynamics simulation of lithiation-induced phase-transition of crystalline silicon, Electrochimica Acta 62 (2012) 73–76.
[37] S.C. Jung, J.W. Choi, Y.-K. Han, Anisotropic volume expansion of crystalline silicon during electrochemical lithium insertion: an atomic level rationale, Nano letters 12 (10) (2012) 5342–5347.
[38] L. Huang, B. Han, B. Han, A. Derecskei-Kovacs, M. Xiao, X. Lei, M.L. O'Neill, R. M. Pearlstein, H. Chandra, H. Cheng, First-principles study of a full cycle of atomic layer deposition of sio_2 thin films with di(sec-butylamino)silane and ozone, J. Phys. Chem. C 117 (38) (2013) 19454–19463.
[39] S.-Y. Kim, Y. Qi, Property evolution of al_2o_3 coated and uncoated si electrodes: a first principles investigation, J. Electrochem. Soc. 161 (11) (2014) F3137–F3143.
[40] K. Leung, First-principles modeling of the initial stages of organic solvent decomposition on lixmn2o4(100) surfaces, J. Phys. Chem. C 116 (18) (2012) 9852–9861.
[41] K. Hankins, F.A. Soto, P.B. Balbuena, Insights into the Li Intercalation and SEI Formation on LiSi Nanoclusters, J. Electrochem. Soc. 164 (11) (2017) E3457–E3464.
[42] D.H. Snydacker, V.I. Hegde, C. Wolverton, Electrochemically stable coating materials for li, na, and mg metal anodes in durable high energy batteries, J. Electrochem. Soc. 164 (14) (2017) A3582–A3589.
[43] A. Wang, S. Kadam, H. Li, S. Shi, Y. Qi, Review on modeling of the anode solid electrolyte interphase (SEI) for lithium-ion batteries, Npj Computational Materials 4 (1) (2018).
[44] Y. Xiao, L.J. Miara, Y. Wang, G. Ceder, Computational screening of cathode coatings for solid-state batteries, Joule 3 (5) (2019) 1252–1275.
[45] S. Mo, B. Zhang, K. Zhang, S. Li, F. Pan, LiAl5O8 as a potential coating material in lithium-ion batteries: a first principles study, Phys. Chem. Chemical Physics 21 (25) (2019) 13758–13765.
[46] Q. He, B. Yu, Z. Li, Y. Zhao, Density functional theory for battery materials, Energy & Environ. Mater. 2 (4) (2019) 264–279.
[47] S.C. Jung, D.S. Jung, J.W. Choi, Y.-K. Han, Atom-Level Understanding of the Sodiation Process in Silicon Anode Material, J. Chem. Phys. Letters 5 (7) (2014) 1283–1288.
[48] A. Ostadhossein, S.-Y. Kim, E.D. Cubuk, Y. Qi, A.C.T. van Duin, Atomic insight into the lithium storage and diffusion mechanism of sio_2/al_2o_3 electrodes of lithium ion batteries: reaxff reactive force field modeling, J. Chem. Phys. A 120 (13) (2016) 2114–2127.
[49] A. Karim, S. Fosse, K.A. Persson, Surface structure and equilibrium particle shape of the $LiMn_2O_4$ spinel from first-principles calculations, Physical Review B 87 (7) (2013), 075322.
[50] G. Kresse, J. Furthmüller, Efficient iterative schemes for ab initio total-energy calculations using a plane-wave basis set, Physical Review B 54 (16) (1996) 11169–11186.
[51] C.-H. An, W. Kang, Q.-B. Deng, N. Hu, Pt and Te codoped ultrathin MoS_2 nanosheets for enhanced hydrogen evolution reaction with wide pH range, Rare Metals 41 (2) (2022) 378–384.
[52] Perdew, J. P.; Burke, K.; Ernzerhof, M., Generalized gradient approximation made simple (vol 77, pg 3865, 1996). *PHYSICAL REVIEW LETTERS* **1997,** *78* (7), 1396-1396.
[53] S.L. Dudarev, G.A. Botton, S.Y. Savrasov, C.J. Humphreys, A.P. Sutton, Electron-energy-loss spectra and the structural stability of nickel oxide: An LSDA+U study, Physical Review B 57 (3) (1998) 1505–1509.
[54] S. Kim, M. Aykol, C. Wolverton, Surface phase diagram and stability of (001) and (111) $LiMn_2O_4$ spinel oxides, Physical Review B 92 (11) (2015), 115411.
[55] J.O. Besenhard, J. Heydecke, E. Wudy, H.P. Fritz, W. Foag, Characteristics of molybdenum oxide and chromium oxide cathodes in primary and secondary organic electrolyte lithium batteries. Part II. Transport properties, Solid State Ionics 8 (1) (1983) 61–71.
[56] A. Van der Ven, J. Bhattacharya, A.A. Belak, Understanding Li diffusion in Li-intercalation compounds, Accounts of chemical research 46 (5) (2013) 1216–1225.
[57] M. Park, X. Zhang, M. Chung, G.B. Less, A.M. Sastry, A review of conduction phenomena in Li-ion batteries, J. Power Sources 195 (24) (2010) 7904–7929.
[58] S.C. Jung, H.-J. Kim, J.W. Choi, Y.-K. Han, Sodium ion diffusion in al_2o_3: a distinct perspective compared with lithium ion diffusion, NANO LETTERS 14 (11) (2014) 6559–6563.
[59] K. Tibbetts, C.R. Miranda, Y.S. Meng, G. Ceder, An ab initio study of lithium diffusion in titanium disulfide nanotubes, Chem. Mater. 19 (22) (2007) 5302–5308.
[60] S. Liu, M. Wang, H. Ji, X. Shen, C. Yan, T. Qian, Altering the rate-determining step over cobalt single clusters leading to highly efficient ammonia synthesis, National Science Review 8 (5) (2021) nwaa136.
[61] S. Hao, C. Wolverton, Lithium Transport in Amorphous Al_2O_3 and AlF_3 for Discovery of Battery Coatings, J. Chem. Phys. C 117 (16) (2013) 8009–8013.
[62] O.A. Dicks, A.L. Shluger, Theoretical modeling of charge trapping in crystalline and amorphous Al_2O_3, J. Phys.-condensed matter 29 (31) (2017) 314005.
[63] G.A. Tritsaris, K. Zhao, O.U. Okeke, E. Kaxiras, Diffusion of lithium in bulk amorphous silicon: a theoretical study, J. Chem. Phys. C 116 (42) (2012) 22212–22216.
[64] H.G. Schimmel, G.J. Kearley, J. Huot, F.M. Mulder, Hydrogen diffusion in magnesium metal (alpha phase) studied by ab initio computer simulations, Journal of alloys and compounds 404 (2005) 235–237.
[65] S.P. Ong, Y. Mo, W.D. Richards, L. Miara, H.S. Lee, G. Ceder, Phase stability, electrochemical stability and ionic conductivity of the Li10±1MP2X12 (M = Ge, Si, Sn, Al or P, and X = O, S or Se) family of superionic conductors, Energy & Environmental Science 6 (1) (2013) 148–156.
[66] B. Sahli, W. Fichtner, Ab initio molecular dynamics simulation of self-interstitial diffusion in silicon, Physical Review B 72 (24) (2005), 245210.
[67] J. Schoiswohl, G. Kresse, S. Surnev, M. Sock, M.G. Ramsey, F.P. Netzer, Planar vanadium oxide clusters: Two-dimensional evaporation and diffusion on Rh(111), Physical Review Letters 92 (20) (2004), 206103.
[68] S. Hocker, F. Gähler, Aluminium diffusion in decagonal quasicrystals, Physical Review Letters 93 (7) (2004), 075901.

[69] G. Cherkashinin, R. Hausbrand, W. Jaegermann, Performance of li-ion batteries: contribution of electronic factors to the battery voltage, J. Electrochem. Soc. 166 (3) (2019) A5308–A5312.
[70] H. Gerischer, F. Decker, B. Scrosati, The electronic and the ionic contribution to the free energy of alkali metals in intercalation compounds, J. Electrochem. Soc. 141 (9) (1994) 2297–2300.
[71] D. White, K.S. Seshadri, D.F. Dever, M.J. Linevsky, D.E. Mann, Infrared spectra and structures and thermodynamics of gaseous lio, li2o, and li2o2, J. Chem. Phys. 39 (10) (1963) 2463–3000.
[72] S.F. Li, H. Lu, P. Li, Z. Yang, Z.X. Guo, First-principles local density approximation (generalized gradient approximation) plus U study of catalytic CenOm clusters: U value differs from bulk, J. Chem. Phys. 128 (16) (2008).
[73] Y. Nagai, T. Nonaka, A. Suda, M. Sugiura, In *Structure Analysis of CeO_2-ZrO_2 Mixed Oxides as Oxygen Storage Promoters in*, Automotive Catalysts (2002).